

# First order ferromagnetic phase transition in the low electronic density regime of a biased graphene bilayer

T. Stauber<sup>1</sup>, Eduardo V. Castro<sup>2</sup>, N. A. P. Silva<sup>1</sup>, and  
N. M. R. Peres<sup>1</sup>

<sup>1</sup>Centro de Física e Departamento de Física, Universidade do Minho, P-4710-057,  
Braga, Portugal

<sup>2</sup> CFP and Departamento de Física, Faculdade de Ciências Universidade do Porto,  
P-4169-007 Porto, Portugal

**Abstract.** The phase diagram of a biased graphene bilayer is computed and the existence of a ferromagnetic phase is discussed both in the critical on-site interaction  $U_c$  versus doping density and versus temperature. We show that in the ferromagnetic phase the two planes have unequal magnetization and that the electronic density is hole like in one plane and electron like in the other. We give evidence for a *first-order* phase transition between paramagnetic and ferromagnetic phases induced by doping at zero temperature.

PACS numbers: 73.20.Hb, 81.05.Uw, 73.20.-r, 73.23.-b

## 1. Introduction

Graphene, a two-dimensional hexagonal lattice of carbon atoms, has attracted considerable attention due to its unusual electronic properties, characterized by massless Dirac Fermions.[1, 2, 3] It was first produced via micromechanical cleavage on top of a SiO<sub>2</sub> substrate[4, 5] and its hallmark is the half integer quantum Hall effect.[6, 7]

In addition to graphene, few-layer graphene can also be produced. Of particular interest to us is the double layer graphene system, where one encounters two carbon layers placed on top of each other according to usual Bernal stacking of graphite (see Fig. 1). The low-energy properties of this so-called bilayer graphene are then described by massive Dirac Fermions.[8] These new quasi-particles have a quadratic dispersion close to the neutrality point and have recently been identified in Quantum Hall measurements[9] and in Raman spectroscopy.[10, 11]

In a graphene bilayer it is possible to have the two planes at different electrostatic potentials.[12, 13] As a consequence, a gap opens up at the Dirac point and the low energy band acquires a Mexican hat relation dispersion.[14] This system is called a biased graphene bilayer. The potential difference created between the two layers can be obtained by applying a back gate voltage to the bilayer system and covering the exposed surface with some chemical dopant, as for example Potassium[12] or NH<sub>3</sub>. [13] In addition, it is also possible to control the potential difference between the layers by using back and top gate setups.[15] The opening of the gap at the Dirac point in the biased bilayer system was demonstrated both by angle resolved photoemission experiments (ARPES)[12] and Hall effect measurements.[13] The electronic gap in the biased system has been also observed in epitaxially grown graphene films on SiC crystal surfaces.[16]

Due to the Mexican hat dispersion relation the density of states close to the gap diverges as the square root of the energy. The possibility of having an arbitrary large density of states at the Fermi energy poses the question whether this system can be unstable toward a ferromagnetic ground state. The question of magnetism in carbon based systems already has a long history. Even before the discovery of graphene, highly oriented pyrolytic graphite (HOPG) has attracted a broad interest due to the observation of anomalous properties, such as magnetism and insulating behavior in the direction perpendicular to the planes. [17, 18, 19, 20, 21] The research of  $s - p$  based magnetism[22, 23, 24] was especially motivated by the technological use of nanosized particles of graphite, which show interesting features depending on their shape, edges, and applied field of pressure.[25]

Microscopic theoretical models of bulk carbon magnetism include nitrogen-carbon compositions where ferromagnetic ordering of spins could exist in  $\pi$  delocalized systems due to a lone electron pair on a trivalent element[26] or intermediate graphite-diamond structures where the alternating  $sp^2$  and  $sp^3$  carbon atoms play the role of different valence elements. [27] More general models focus on the interplay between disorder and interaction. [28, 29] Further, midgap states due to zig-zag edges play a

predominant role in the formation of magnetic moments [30, 31] which support flat-band ferromagnetism.[32, 33, 34] A generic model based on midgap states was recently proposed in Refs. [35, 36]. Magnetism is also found in fullerene based metal-free systems.[37] For a recent overview on metal-free Carbon-based magnetism see Ref. [38].

To understand carbon-based magnetism in graphite, one may start with the simplest case of one-layer, i.e., graphene. Because the density of states of intrinsic graphene vanishes at the Dirac point, the simple Stoner-like argument predicts an arbitrary large value of the Coulomb on-site energy needed to produce a ferromagnetic ground state.[39, 40] In fact, because of the vanishing density of states, the Coulomb interaction is not screened and the Hubbard model is not a good starting point to study ferromagnetism in clean graphene. One, therefore, has to consider the exchange instability of the Dirac gas due to the bare, long-range Coulomb interaction in two dimensions. This study shows that for a clean, doped or undoped graphene layer, a spin-polarized ground-state due to the gain of exchange energy is only favorable for unphysical values of the dimensionless coupling constant of graphene.[41] The paramagnetic ground-state of clean graphene is thus stable against the exchange interaction. If the system is disordered, e.g., due to vacancies or edge states, a finite density of states builds in at the Dirac point. As a consequence, a finite Hubbard interaction for driving the system to a ferromagnetic ground state is obtained.[42] In this case, the exchange interaction favors a ferromagnetic ground state for reasonable values of the dimensionless coupling parameter.[41] The presence of itinerant magnetism due to quasi-localized states induced by single-atom defects in graphene, such as vacancies,[43] has also been obtained recently using first-principles.[44]

The situation is quite different in a bilayer system. There, a finite density of states exists at the neutrality point producing some amount of screening in the system. Moreover, in the case of a biased bilayer and for densities close to the energy gap, the density of states is very large producing very effective screening. As a consequence, for this system the Hubbard model is a good starting point to study the tendency toward ferromagnetism. From the point of view of the exchange instability of the bilayer system, it is found that the system is always unstable toward a ferromagnetic ground state for low enough particle densities. [45, 46, 47]

In the present paper, we want to explore the fact that the Hubbard model is a good starting point to describe the Coulomb interactions in the regime where the Fermi energy is close to the band edge of the biased bilayer system. In particular we want to study the phase diagram of the system as function of the doping. We further want to determine the mean field critical temperature.

The paper is organized as followed. In section 2, we introduce the model and define the mean-field decoupling which allows for different electronic density and magnetization in the two layers. In section 3, we set up the mean-field equations and present the numerical results in section 4. We close with conclusions and future research directions.

## 2. Model Hamiltonian and mean field approximation

The Hamiltonian of a biased bilayer Hubbard model is the sum of two pieces  $H = H_{TB} + H_U$ , where  $H_{TB}$  is the tight-binding part and  $H_U$  is the Coulomb on-site interaction part of the Hamiltonian. The tight-binding Hamiltonian is itself a sum of four terms describing the tight-binding Hamiltonian of each plane, the hopping term between the planes, and the electrostatic bias applied to the two planes. We therefore have,

$$H_{TB} = \sum_{\iota=1}^2 H_{TB,\iota} + H_{\perp} + H_V, \quad (1)$$

with

$$H_{TB,\iota} = -t \sum_{\mathbf{R},\sigma} [a_{\iota\sigma}^{\dagger}(\mathbf{R})b_{\iota\sigma}(\mathbf{R}) + a_{\iota\sigma}^{\dagger}(\mathbf{R})b_{\iota\sigma}(\mathbf{R} - \mathbf{a}_1) + a_{\iota\sigma}^{\dagger}(\mathbf{R})b_{\iota\sigma}(\mathbf{R} - \mathbf{a}_2) + H.c.], \quad (2)$$

$$H_{\perp} = -t_{\perp} \sum_{\mathbf{R},\sigma} [a_{1\sigma}^{\dagger}(\mathbf{R})b_{2\sigma}(\mathbf{R}) + b_{2\sigma}^{\dagger}(\mathbf{R})a_{1\sigma}(\mathbf{R})], \quad (3)$$

and

$$H_V = \frac{V}{2} \sum_{\mathbf{R},\sigma} [n_{a1\sigma}(\mathbf{R}) + n_{b1\sigma}(\mathbf{R}) - n_{a2\sigma}(\mathbf{R}) - n_{b2\sigma}(\mathbf{R})]. \quad (4)$$

As regards the bias term in Eq. (4), we assume here that  $V$  can be externally controlled and is independent of the charge density in the system. This situation can be realized with a back and top gate setup.[15] The on-site Coulomb part is given by,

$$H_U = U \sum_{\mathbf{R}} [n_{a1\uparrow}(\mathbf{R})n_{a1\downarrow}(\mathbf{R}) + n_{b1\uparrow}(\mathbf{R})n_{b1\downarrow}(\mathbf{R}) + n_{a2\uparrow}(\mathbf{R})n_{a2\downarrow}(\mathbf{R}) + n_{b2\uparrow}(\mathbf{R})n_{b2\downarrow}(\mathbf{R})], \quad (5)$$

where  $n_{x\iota\sigma}(\mathbf{R}) = x_{\iota\sigma}^{\dagger}(\mathbf{R})x_{\iota\sigma}(\mathbf{R})$ , with  $x = a, b$ ,  $\iota = 1, 2$  and  $\sigma = \uparrow, \downarrow$ .

The problem defined by the Hamiltonian  $H_{TB} + H_U$  can not be solved exactly and therefore we have to rest upon some approximation. Here we adopt a mean field approach, neglecting quantum fluctuations. Since we are interested in studying the existence of a ferromagnetic phase we have to introduce a broken symmetry ground state. There is however an important point to remark: since the two planes of the bilayer are at different electrostatic potentials one should expect that the electronic density and the magnetization will not be evenly distributed among the two layers. Therefore our broken symmetry ground state must take this aspect into account. As a consequence we propose the following broken symmetry ground state:

$$\langle n_{x1\sigma}(\mathbf{R}) \rangle = \frac{n + \Delta n}{8} + \sigma \frac{m + \Delta m}{8}, \quad (6)$$

and

$$\langle n_{x2\sigma}(\mathbf{R}) \rangle = \frac{n - \Delta n}{8} + \sigma \frac{m - \Delta m}{8}, \quad (7)$$

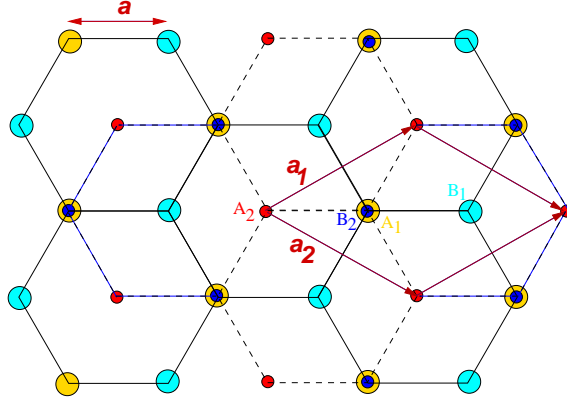


**Figure 1.** (Color online) The unit cell  $a$  of graphene bilayer in the Bernal stacking. The dashed hexagons are on top of the solid ones. The unit cell vectors have coordinates  $\mathbf{a}_1 = a(3, \sqrt{3})/2$  and  $\mathbf{a}_2 = a(3, -\sqrt{3})/2$ .

where  $n$  is the density per unit cell and  $m = n_\uparrow - n_\downarrow$  is the spin polarization per unit cell. The quantities  $\Delta n$  and  $\Delta m$  represent the difference in the electronic density and in the spin polarization between the two layers, respectively.[48] We note that  $m$  and  $\Delta m$  are independent parameters, being in principle possible to have a ground state where  $m = 0$  but  $\Delta m \neq 0$ .

When transformed to momentum space the mean field Hamiltonian obtained from the above reads

$$\begin{aligned}
 H_{MF} &= \sum_{\mathbf{k}, \sigma} \Psi_{\mathbf{k}, \sigma}^\dagger H_{\mathbf{k}, \sigma} \Psi_{\mathbf{k}, \sigma} \\
 &- \frac{N_c U}{32} [(n + \Delta n)^2 - (m + \Delta m)^2] \\
 &- \frac{N_c U}{32} [(n - \Delta n)^2 - (m - \Delta m)^2], \tag{8}
 \end{aligned}$$

with  $\Psi_{\mathbf{k}, \sigma}^\dagger = [a_{1\mathbf{k}\sigma}^\dagger, b_{1\mathbf{k}\sigma}^\dagger, a_{2\mathbf{k}\sigma}^\dagger, b_{2\mathbf{k}\sigma}^\dagger]$  and  $H_{\mathbf{k}, \sigma}$  given by

$$H_{\mathbf{k}, \sigma} = \begin{pmatrix} s_\sigma & -t\phi_{\mathbf{k}} & 0 & -t_\perp \\ -t\phi_{\mathbf{k}}^* & s_\sigma & 0 & 0 \\ 0 & 0 & p_\sigma & -t\phi_{\mathbf{k}} \\ -t_\perp & 0 & -t\phi_{\mathbf{k}}^* & p_\sigma \end{pmatrix}, \tag{9}$$

with  $s_\sigma = \frac{V}{2} + \left(\frac{n+\Delta n}{8} - \sigma \frac{m+\Delta m}{8}\right) U$ ,  $p_\sigma = -\frac{V}{2} + \left(\frac{n-\Delta n}{8} - \sigma \frac{m-\Delta m}{8}\right) U$ , and  $\phi_{\mathbf{k}} = 1 + e^{i\mathbf{k}\cdot\mathbf{a}_1} + e^{i\mathbf{k}\cdot\mathbf{a}_2}$ . The energy eigenvalues are given by,

$$\begin{aligned}
 E_\sigma^{j,l}(\mathbf{k}, m, \Delta m) &= \left(\frac{n}{8} - \sigma \frac{m}{8}\right) U \\
 &+ \frac{l}{2} \sqrt{2t_\perp^2 + V_\sigma^2 + 4t^2|\phi_{\mathbf{k}}|^2 + j2\sqrt{t_\perp^4 + 4t^2(t_\perp^2 + V_\sigma^2)}|\phi_{\mathbf{k}}|^2}, \tag{10}
 \end{aligned}$$

where  $l, j = \pm$  and  $V_\sigma$  is given by

$$V_\sigma = V + U\Delta\tilde{n} - \sigma U\Delta\tilde{m}, \tag{11}$$

where we have introduced the definitions  $\Delta n = 4\Delta\tilde{n}$  and  $\Delta m = 4\Delta\tilde{m}$ . It is clear that as long as  $\Delta n$  and  $\Delta m$  are finite the system has an effective  $V_\sigma$  that differs from the bare value  $V$ . The momentum values are given by,

$$\mathbf{k} = \frac{m_1}{N}\mathbf{b}_1 + \frac{m_2}{N}\mathbf{b}_2, \quad (12)$$

with  $m_1, m_2 = 0, 1, \dots, N-1$ , the number of unit cells given by  $N_c = N^2$ , and  $\mathbf{b}_1$  and  $\mathbf{b}_2$  given by,

$$\mathbf{b}_1 = \frac{2\pi}{3a}(1, \sqrt{3}), \quad \mathbf{b}_2 = \frac{2\pi}{3a}(1, -\sqrt{3}). \quad (13)$$

The Brillouin zone of the system is represented in Fig. 2.

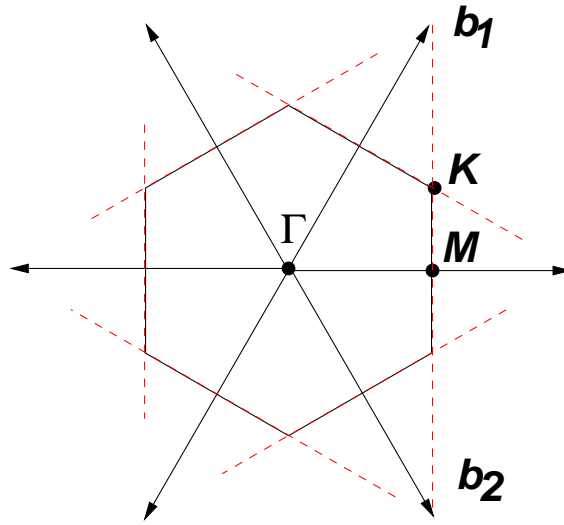


**Figure 2.** (Color online) Brillouin zone of the bilayer problem. The Dirac point  $\mathbf{K}$  has coordinates  $2\pi(1, \sqrt{3}/3)/(3a)$  and the  $\mathbf{M}$  point has coordinates  $2\pi(1, 0)/(3a)$ .

### 3. Free energy and mean-field equations

The free energy per unit cell,  $f$ , of Hamiltonian (8) is given by,

$$f = -\frac{k_B T}{N_c} \sum_{\mathbf{k}, \sigma} \sum_{l, j=\pm} \ln \left( 1 + e^{-(E_\sigma^{l,j}(\mathbf{k}) - \mu)/(k_B T)} \right) - \frac{U}{16} [n^2 - m^2 + (\Delta n)^2 - (\Delta m)^2] + \mu n, \quad (14)$$

where  $\mu$  is the chemical potential.

Let us introduce the density of states per spin per unit cell  $\rho(E)$  defined as

$$\rho(E) = \frac{1}{N_c} \sum_{\mathbf{k}} \delta(E - t|\phi_{\mathbf{k}}|). \quad (15)$$

The momentum integral in Eq. (15) is over the Brillouin zone defined in Fig. 2, using the momentum definition (12). The integral can be performed leading to,

$$\rho(E) = \frac{2E}{t^2\pi^2} \begin{cases} \frac{1}{\sqrt{F(E/t)}} \mathbf{K} \left( \frac{4E/t}{F(E/t)} \right), & 0 < E < t, \\ \frac{1}{\sqrt{4E/t}} \mathbf{K} \left( \frac{F(E/t)}{4E/t} \right), & t < E < 3t, \end{cases} \quad (16)$$

where  $F(x)$  is given by

$$F(x) = (1+x)^2 - \frac{(x^2-1)^2}{4}, \quad (17)$$

and  $\mathbf{K}(m)$  is defined as,

$$\mathbf{K}(m) = \int_0^1 dx [(1-x^2)(1-mx^2)]^{-1/2}. \quad (18)$$

Using Eq. (15), the free energy in Eq. (15) can be written as a one-dimensional integral,

$$\begin{aligned} f = & \\ & -k_B T \sum_{\sigma} \sum_{l,j=\pm} \int dE \rho(E) \ln \left( 1 + e^{-(E_{\sigma}^{l,j}(E) - \mu)/(k_B T)} \right) \\ & - \frac{U}{16} [n^2 - m^2 + (\Delta n)^2 - (\Delta m)^2] + \mu n. \end{aligned} \quad (19)$$

The mean field equations are now obtained from the minimization of the free energy (19). The doping,  $\delta n$ , relative to the situation where the system is at half filling is defined as,

$$\delta n = \sum_{\sigma} \sum_{l,j=\pm} \int dE \rho(E) f[E_{\sigma}^{l,j}(E) - \mu] - 4, \quad (20)$$

where  $f(x) = (1 + e^{x/(k_B T)})^{-1}$ . The spin polarization per unit cell obeys the mean field equation,

$$m = \sum_{\sigma} \sum_{l,j=\pm} \sigma \int dE \rho(E) f[E_{\sigma}^{l,j}(E) - \mu]. \quad (21)$$

The difference in the electronic density between the two layers is obtained from,

$$\Delta \tilde{n} = \frac{1}{2} \sum_{\sigma} \sum_{l,j=\pm 1} \int dE \rho(E) f[E_{\sigma}^{l,j}(E) - \mu] v_{\sigma}^{l,j}(E), \quad (22)$$

where  $v_{\sigma}^{l,j}(E)$  is given by

$$v_{\sigma}^{l,j}(E) = \frac{l}{2} \frac{V_{\sigma}}{\sqrt{\dots}} \left( 1 + \frac{j4E^2}{\sqrt{t_{\perp}^4 + 4E^2(t_{\perp}^2 + V_{\sigma}^2)}} \right), \quad (23)$$

and

$$\sqrt{\dots} = \sqrt{2t_{\perp}^2 + V_{\sigma}^2 + 4E^2 + j2\sqrt{t_{\perp}^4 + 4E^2(t_{\perp}^2 + V_{\sigma}^2)}}. \quad (24)$$

The difference in the magnetization between the two layers is obtained from

$$\Delta\tilde{m} = \frac{1}{2} \sum_{\sigma} \sum_{l,j=\pm 1} \sigma \int dE \rho(E) f[E_{\sigma}^{l,j}(E) - \mu] v_{\sigma}^{l,j}(E), \quad (25)$$

Let us now assume that the system supports a ferromagnetic ground state whose magnetization vanishes at some critical value  $U_c$  at zero temperature. Additionally we assume that  $\Delta m = 0$  when  $m = 0$ , which will be shown to be the case in this system. The value of  $U_c$  is determined from expanding (21) to first order in  $m$ , leading to,

$$\begin{aligned} 1 &= \frac{U_c}{4} \sum_{l,j=\pm 1} \int dE \rho(E) \delta[E_{\sigma}^{l,j}(E, 0, 0) - \mu] \\ &= \frac{U_c}{4} \sum_{l,j,k=\pm 1}^* \frac{\rho(E_k^*)}{|f'_{l,j}(E_k^*)|} \theta(3t - E_k^*) \theta(E_k^*) \\ &= \frac{U_c}{4} \rho_b(\tilde{\mu}, U_c) = U_c \tilde{\rho}_b(\tilde{\mu}, U_c), \end{aligned} \quad (26)$$

where  $\rho_b(\tilde{\mu}, U_c)$  is the density of states per unit cell per spin for a biased bilayer at the energy  $\tilde{\mu} = \mu - nU_c/8$  and  $\tilde{\rho}_b(\tilde{\mu}, U_c)$  is the density of states per spin per lattice point. Although Eq. (26) looks like the usual Stoner criterion the fact that the bias  $V_{\sigma}$  given in Eq. (11) depend on  $U$  due to the difference in the electronic density  $\Delta n$  makes Eq. (26) a non-linear equation for  $U_c$  which must be solved self-consistently. For low doping  $\delta n$  the product  $U_c \Delta \tilde{n}$  is a small number when compared to  $V$  and therefore it can be neglected in Eq. (11). In this case Eq. (26) reduces to the usual Stoner criterion:

$$U_c \simeq 1/[\tilde{\rho}_b(\tilde{\mu})]. \quad (27)$$

The quantities  $E_k^*$  in Eq. (26) are the roots of the delta function argument,

$$E_{\sigma}^{l,j}(E_k^*) - \mu = 0. \quad (28)$$

The quantity  $f'_{l,j}(E_k^*)$  is the derivative in order to the energy  $E$  of Eq. (28) evaluated at the roots  $E_k^*$ . The roots  $E_k^*$  are given by

$$E_k^* = \frac{1}{2} \sqrt{4\tilde{\mu}^2 + V_{\sigma}^2 + k2\sqrt{4\tilde{\mu}^2(t_{\perp}^2 + V_{\sigma}^2) - t_{\perp}^2 V_{\sigma}^2}}, \quad (29)$$

with  $k = \pm$ . Equation (28) cannot be solved for all bands: the existence of a solution is determined by  $\mu$ . As a consequence we added the  $*$  symbol in the summation of Eq. (26), which means that only bands for which Eq. (28) can be solved (two at the most) contribute to the summation. It also means that for the contributing bands only real roots in Eq. (29) are taken into account to the summation. The number of real roots in Eq. (29) depends on the particular band an  $\mu$  through Eq. (28). As the function  $f'_{l,j}(E)$  is given by

$$f'_{l,j}(E) = \frac{2lE}{\sqrt{\dots}} \left( 1 + j \frac{t_{\perp}^2 + V_{\sigma}^2}{\sqrt{t_{\perp}^4 + 4E^2(t_{\perp}^2 + V_{\sigma}^2)}} \right). \quad (30)$$

it is clear that both roots are imaginary for  $\tilde{\mu}$  in the range

$$-\frac{t_{\perp} V_{\sigma}}{2\sqrt{t_{\perp}^2 + V_{\sigma}^2}} < \tilde{\mu} < \frac{t_{\perp} V_{\sigma}}{2\sqrt{t_{\perp}^2 + V_{\sigma}^2}}, \quad (31)$$



which means that the system has an energy gap of value

$$\Delta_g = \frac{t_\perp V_\sigma}{\sqrt{t_\perp^2 + V_\sigma^2}}. \quad (32)$$

We finally note that since we have assumed  $\Delta m = 0$ ,  $V_\sigma$  does not effectively depend on  $\sigma$ .

## 4. Results and Discussion

We start with the zero temperature phase diagram in the plane  $U$  vs.  $\delta n$ . An approximate analytic treatment is possible in this limit, which is used to check our numerical results. The effect of temperature is considered afterwards.

### 4.1. Zero temperature

*4.1.1. Approximate solution* In Fig. 3 we represent the density of states of a biased bilayer with  $U = 0$  together with the low doping critical value  $U_c$ , as given by Eq. (27). In panel (b) of Fig. 3 a zoom in of the density of states close to the gap is shown. It is clear that the density of states diverges at the edge of the gap. As consequence the closer to edge of the gap the chemical potential is the lower will be the critical  $U_c$  value. This quantity is shown in panel (c) of Fig. 3 as function of the chemical potential  $\tilde{\mu}$  and in panel (d) as a function of doping  $\delta n$ . The lowest represented value of  $U_c$  is about  $U_c \simeq 2.7$  eV to which corresponds an electronic doping density  $\delta n \simeq 2.5 \times 10^{-5}$  electrons per unit cell. The step like discontinuity shown in panels (c) and (d) for  $U_c$  occurs when the Fermi energy equals  $V/2$ , signaling the top of the Mexican hat dispersion relation.

It is clear from panel (d) of Fig. 3 that in the low doping limit  $U_c$  is a linear function of doping  $\delta n$ . This limit enables for an approximate analytic treatment which not only explains the linear behavior but also provides a validation test of our numerical results. Firstly we note that for very low doping the density of states in Eq. (27) is close to the gap edge,  $|\tilde{\mu}| \sim \Delta_g/2$ , where  $\Delta_g$  is the size of the gap Eq. (32). In this energy region the density of states has a 1D like divergence,[14] behaving as,

$$\rho_b(\tilde{\mu}) \propto \frac{1}{\sqrt{|\tilde{\mu}| - \Delta_g/2}}. \quad (33)$$

Using this approximate expression to compute the doping,  $\delta n \propto \text{sign}(\tilde{\mu}) \times \int_{\Delta_g/2}^{|\tilde{\mu}|} dx \rho_b(x)$ , we immediately get  $\delta n \propto \text{sign}(\tilde{\mu})/\rho_b(\tilde{\mu})$  and thus  $U_c \propto |\delta n|$ . In order to have an analytic expression for  $U_c$  in the low doping limit we have to take into account the proportionality coefficient in Eq. (33). After some algebra it can be shown that the density of states per spin per lattice point near the gap edge can be written as,

$$\rho_b(\tilde{\mu}) \approx \frac{1}{t^2 4\pi^2} \sqrt{\frac{\Delta_g(t_\perp^2 + V^2)}{F(\chi)}} \mathbf{K} \left( \frac{4\chi}{F(\chi)} \right) \frac{1}{\sqrt{|\tilde{\mu}| - \Delta_g/2}}, \quad (34)$$

where  $\chi = [(\Delta_g^2 + V^2)/(4t^2)]^{1/2}$ , with  $F(x)$  and  $\mathbf{K}(m)$  as in Eqs. (17) and (18). The doping  $\delta n$ , measured with respect to half filling in units of electrons per unit cell, can

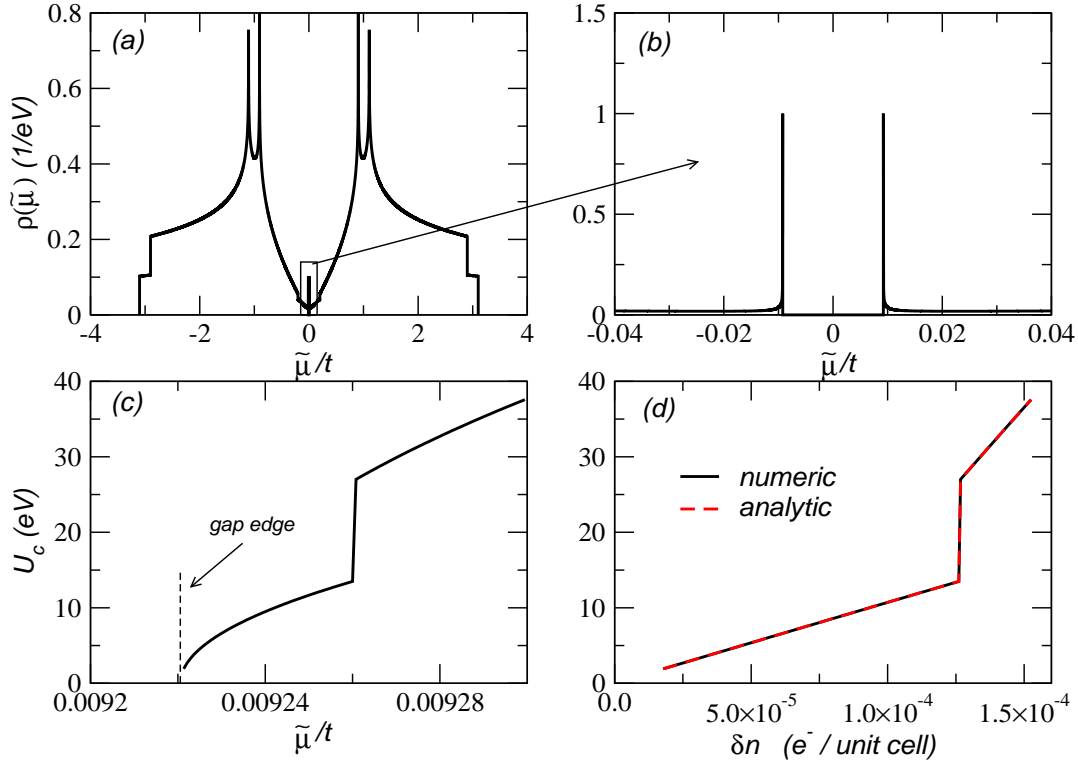


**Figure 3.** (Color online) (a) – Density of states  $\rho(\tilde{\mu})$  per unit cell per spin of the bilayer problem with  $U = 0$ . (b) – Zoom of (a) near the gap region. (c) – Critical value  $U_c$  for ferromagnetism in the low doping,  $\delta n$ , regime. (d) – The same as in (c) as a function of doping. The parameters are  $t = 2.7$  eV,  $t_{\perp} = 0.2t$ ,  $V = 0.05$  eV. The edge of the gap is located at  $\Delta_g/(2t) \simeq 0.00922$ .

be written as,

$$\begin{aligned} \delta n &= \text{sign}(\tilde{\mu}) \times 8 \int_{\Delta_g/2}^{|\tilde{\mu}|} dx \rho_b(x) \\ &\approx \frac{4}{t^2 \pi^2} \sqrt{\frac{\Delta_g(t_{\perp}^2 + V^2)}{F(\chi)}} \mathbf{K} \left( \frac{4\chi}{F(\chi)} \right) \sqrt{|\tilde{\mu}| - \Delta_g/2}. \end{aligned} \quad (35)$$

Inserting Eq. (34) into Eq. (27), and taking into account Eq. (35), we are able to write,

$$U_c \approx t^4 \pi^4 \frac{F(\chi)}{\Delta_g(t_{\perp}^2 + V^2)} \left[ \mathbf{K} \left( \frac{4\chi}{F(\chi)} \right) \right]^{-2} \delta n. \quad (36)$$

In panel (d) of Fig. 3 both the numerical result of Eq. (27) and the analytical result of Eq. (36) are shown. The agreement is excellent.

*4.1.2. Self-consistent solution* We now need to solve the mean field equations in order to obtain the zero temperature phase diagram of the biased bilayer. In order to achieve this goal we study how  $m$ ,  $\Delta m$ , and  $\Delta n$  depend on the interaction  $U$ , for given values of the electronic doping  $\delta n$ .

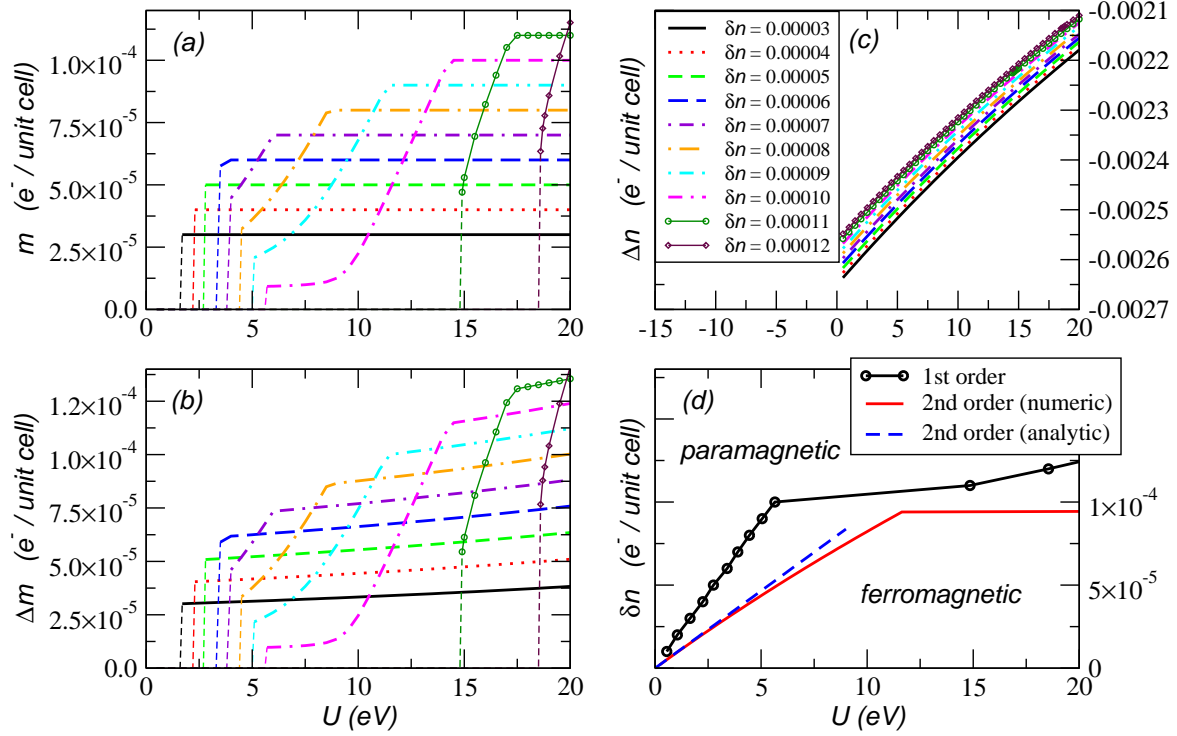


**Figure 4.** (Color online) Panels (a), (b), and (c) show the zero temperature self-consistent solution for  $m$ ,  $\Delta m$ , and  $\Delta n$ , respectively. The zero temperature phase diagram of the biased bilayer in the  $U$  vs.  $\delta n$  plane is shown in panel (d). Symbols in panel (d) are inferred from panel (a) and signal a *first-order* phase transition; the solid [Eq. (26)] and dashed [Eq. (36)] lines stand for a *second-order* phase transition. The constant parameters are  $V = 0.05$  eV,  $t_{\perp} = 0.2t$ , and  $t = 2.7$  eV.

In panel (a) of Fig. 4 it is shown how  $m$  depends on  $U$  for different values of  $\delta n$ . The chosen values of  $\delta n$  correspond to the chemical potential being located at the divergence of the low energy density of states. The lower the  $\delta n$  is the more close to the gap edge is the chemical potential and therefore the larger the density of states is. As a consequence,  $m$  presents a smaller critical  $U_c$  value for smaller  $\delta n$  values. It is interesting to note that the magnetization saturation values correspond to full polarization of the doping charge density with  $m = \delta n$ , also found within a one-band model.[46] In panel (b) of Fig. 4 we plot the  $\Delta m$  mean field parameter. Interestingly the value of  $\Delta m$  vanishes at the same  $U_c$  as  $m$ . For finite values of  $m$  we have  $\Delta m > m$ , which means that the magnetization of the two layers is opposite. We therefore have two ferromagnetic planes that possess opposite and unequal magnetization. In panel (c) of Fig. 4 we show the value of  $\Delta n$  as function of  $U$ . It is clear that  $|\delta n| < |\Delta n|$ , which implies that the density of charge carriers is above the Dirac point in one plane and below it in the other plane. This means that the charge carriers are electron like in one plane and hole like in the other.

In panel (d) of Fig. 4 we show the phase diagram of the system in the  $U$  vs.  $\delta n$  plane. Symbols are inferred from the magnetization behavior in panel (a). They signal a *first-order* phase transition when  $m$  increases from zero to a finite value [see panel (a)]. The

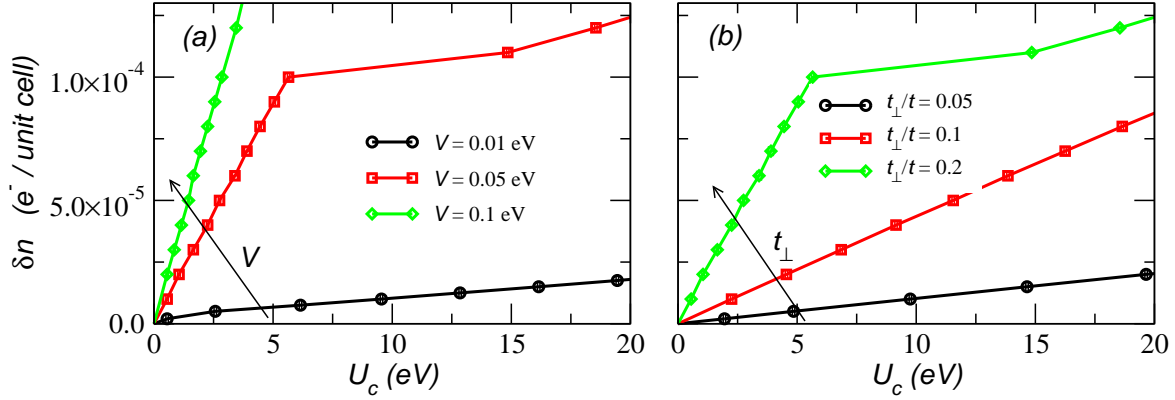


**Figure 5.** (Color online) Effect of  $t_\perp$  and  $V$  on the zero temperature  $U_c$  vs.  $\delta n$  phase diagram: (a) fixed  $t_\perp = 0.2t$  and varying  $V$ ; (b) fixed  $V = 0.05$  eV and varying  $t_\perp$ . For a given  $\delta n$  the *ferromagnetic* phase establishes for  $U > U_c$  and the *paramagnetic* phase for  $U < U_c$ .

full (red) line is the numerical self-consistent result of Eq. (26), and the dashed (blue) line is the approximate analytic result given by Eq. (36). The discrepancy between lines and symbols has a clear meaning. In order to obtain both Eqs. (26) and (27) we assumed that a *second-order* phase transition would take place, i.e., the magnetization  $m$  would vanish continuously when some critical  $U_c$  is approached from above. This is not the case, and the system undergoes a first-order phase transition for smaller  $U$  values than those for the second-order phase transition case. There are clearly two different regimes in panel (d) of Fig. 4: one at densities lower than  $\delta n \lesssim 1 \times 10^{-4}$ , where the dependence of  $\delta n$  on  $U_c$  is linear, and another regime for  $\delta n > 1 \times 10^{-4}$  where a plateau like behavior develops. This plateau has the same physical origin as the step like discontinuity we have seen in panels (c) and (d) of Fig. 3. Clearly, as the density  $\delta n$  grows the needed value of  $U_c$  for having a ferromagnetic ground state increases. This is a consequence of the diverging density of states close to the gap edge. As regards the limit  $\delta n \rightarrow 0$  it is obvious from panel (d) of Fig. 4 that we have  $U_c \rightarrow 0$ . It should be noted, however, that lowering the density  $\delta n$  leads to a decrease of  $m$  and  $\Delta m$ , as can be seen in panels (a) and (b) of Fig. 4. Therefore, even though we have  $U_c \rightarrow 0$  in the limit  $\delta n \rightarrow 0$ , we have also  $m \rightarrow 0$  and  $\Delta m \rightarrow 0$ , which implies a *paramagnetic* ground state for the undoped ( $\delta n = 0$ ) biased bilayer. Only  $\Delta n$  remains finite at zero doping, in agreement with the observations that screening is still possible at the neutrality point ( $\delta n = 0$ ). [49, 13, 50]

So far we have analyzed the system for fixed values of the bias voltage,  $V$ , and interlayer coupling,  $t_\perp$ . In Fig. 5 we show the effect of the variation of these two parameters on the zero temperature phase diagram. In panel (a) we have fixed the interlayer coupling,  $t_\perp = 0.2t$ , and varied the bias voltage,  $V(\text{eV}) = \{0.01, 0.05, 0.1\}$ ; in panel (b) we did the opposite, with  $V = 0.05$  eV and  $t_\perp/t = \{0.05, 0.1, 0.2\}$ . Essentially, raising either  $V$  or  $t_\perp$  leads to a decrease of the critical interaction,  $U_c$ , needed to establish the ferromagnetic phase for a given  $\delta n$ . The order of the transition, however, remains *first-order*: for a given  $\delta n$ , the critical interaction  $U_c$  predicted by Eq. (26), which is

valid for a *second-order* phase transition, is always higher than what is obtained by solving self-consistently the mean-field equations, meaning that a *first-order* transition is occurring at a lower  $U_c$ . It is interesting to note that the effect of  $V$  and  $t_\perp$  on the *first-order* critical  $U_c$  line is similar to what is expected for the usual Stoner criterion, where increasing either  $V$  or  $t_\perp$  gives rise to an increase in the density of states at the Fermi level and a lower  $U_c$  thereof.

The bias voltage and the interlayer coupling have also interesting effects on the magnetization,  $m$ , and spin polarization difference between layers,  $\Delta m$ . Decreasing  $t_\perp$  leads to a decrease in  $\Delta m$ , and below some  $t_\perp$  we have  $\Delta m < m$ , as opposed to the case discussed above ( $V = 0.05$  eV and  $t_\perp = 0.2t$ ). In particular, for  $V = 0.05$  eV, we have already found  $\Delta m < m$  for  $t_\perp \leq 0.1t$ . A similar effect has been observed when  $V$  is increased. For  $t_\perp = 0.2t$  we have found  $\Delta m < m$  for  $V \geq 0.1$  eV. It should be noted, however, that  $m$  and  $\Delta m$  are  $U$ -dependent. Increasing  $U$  leads  $m$  to saturate while  $\Delta m$  keeps growing, as can be seen in panels (a) and (b) of Fig. 4 for the particular case of  $V = 0.05$  eV and  $t_\perp = 0.2t$ . This means that, depending on the value of the parameters  $V$  and  $t_\perp$ , we can go from  $\Delta m < m$  to  $\Delta m > m$  just by increasing the interaction strength  $U$ . It can also be seen in panel (a) of Fig. 4 that  $m$  is completely saturated at the transition for  $\delta n < \delta n_c \approx 6 \times 10^{-5}$  electrons per unit cell, while for  $\delta n > \delta n_c$  it saturates only at some  $U > U_c$ . Even though this behavior seems to be general for any  $V$  and  $t_\perp$ , the value of  $\delta n_c$  is not. In particular, we have found  $\delta n_c$  to depend strongly on  $V$  – it seems to vary monotonically with  $V$ , increasing when  $V$  increases. Let us finally comment on the effect of  $V$  and  $t_\perp$  on the charge imbalance between planes,  $\Delta n$ . Irrespective of  $V$  and  $t_\perp$  we have always observed  $|\delta n| < |\Delta n|$ , which means that charge carriers are always electron like in one plane and hole like in the other. As expected, increasing/decreasing either  $V$  or  $t_\perp$  leads to an increase/decrease of  $\Delta n$ .

*4.1.3. Understanding the asymmetry between planes* The asymmetry between planes regarding both charge and spin polarization densities can be understood based on the Hartree-Fock bands shown in Fig. 6. The figure stands for  $V = 0.05$  eV and  $t_\perp = 0.2t$ , but can easily be generalized for other parameter values.

It should be noted firstly that in the biased bilayer the weight of the wave functions in each layer for near-gap states is strongly dependent on their valence band or conduction band character.[13, 49, 50] Valence band states near the gap have their amplitude mostly localized on layer 2, due to the lower electrostatic potential  $-V/2$  [see Eq. (4)]. On the other hand, near-gap conduction band states have their highest amplitude on layer 1, due to the higher electrostatic potential  $+V/2$  for this layer [see Eq. (4)].

The case  $U < U_c$  shown in Fig. 6 (left) stands for the paramagnetic phase. The values  $m = 0$  and  $\Delta m = 0$  seen in this phase are an immediate consequence of the degeneracy of *up* and *down* spin polarized bands. The presence of a finite gap, however, leads to the abovementioned asymmetry between near-gap valence and conduction states. As a consequence, a half-filled bilayer would have  $n_2 = (4 + \Delta n)/2$  electrons per

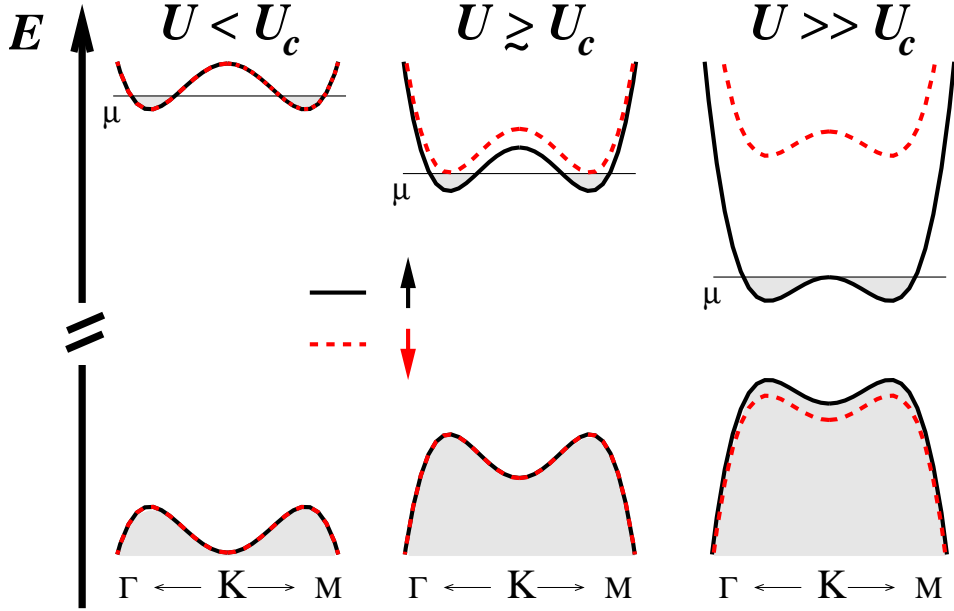


**Figure 6.** (Color online) Hartree-Fock bands for *up* (full lines) and *down* (dashed lines) spin polarizations. Three different cases are considered (from left to right):  $U < U_c$ ,  $U \gtrsim U_c$ , and  $U \gg U_c$ .

unit cell on layer 2 (electron like charge carriers) and  $n_1 = (4 - \Delta n)/2$  electrons per unit cell on layer 1 (hole like charge carriers), with  $\Delta n \neq 0$ . Even though the system studied here is not at half-filling, as long as  $|\delta n| < |\Delta n|$  the carriers on layers 1 and 2 will still be hole and electron like, respectively. Note that as  $U$  is increased the charge imbalance  $\Delta n$  is suppressed in order to reduce the system Coulomb energy, as can be seen in panel (c) of Fig. 4. From the band structure point of view a smaller  $\Delta n$  is the result of a smaller gap  $\Delta_g$ , which means that increasing  $U$  has the effect of lowering the gap.

Let us now consider the case  $U \gtrsim U_c$  shown in Fig. 6 (center). The degeneracy lifting of spin polarized bands gives rise to a finite magnetization,  $m \neq 0$ . Interestingly enough, the degeneracy lifting is only appreciable for conduction bands, as long as  $U$  is not much higher than  $U_c$ . This explains why the total polarization  $m$  and the difference in polarization between layers  $\Delta m$  have similar values,  $m \approx \Delta m$ , as shown in panels (a) and (b) of Fig. 4 – as only conduction bands are contributing to  $\Delta m$ , the spin polarization density is almost completely localized in layer 1, where  $m_1 = (m + \Delta m)/2 \approx m$ , while the spin polarization in layer 2 is negligible,  $m_2 = (m - \Delta m)/2 \approx 0$ .

It is only when  $U \gg U_c$  that valence bands become non-degenerate, as seen in Fig. 6 (right). This implies that near-gap valence states with *up* and *down* spin polarization have different amplitudes in layer 2. As the valence band for *down* spin polarization has a lower energy the near-gap valence states with spin *down* have higher amplitude in layer 2 than their spin *up* counterparts. Consequently, the magnetization in layer 2 is effectively opposite to that in layer 1, i.e.,  $\Delta m > m$ . This can be observed in panels (a) and (b) of Fig. 4, where as  $U$  is increased the magnetization of the two layers becomes

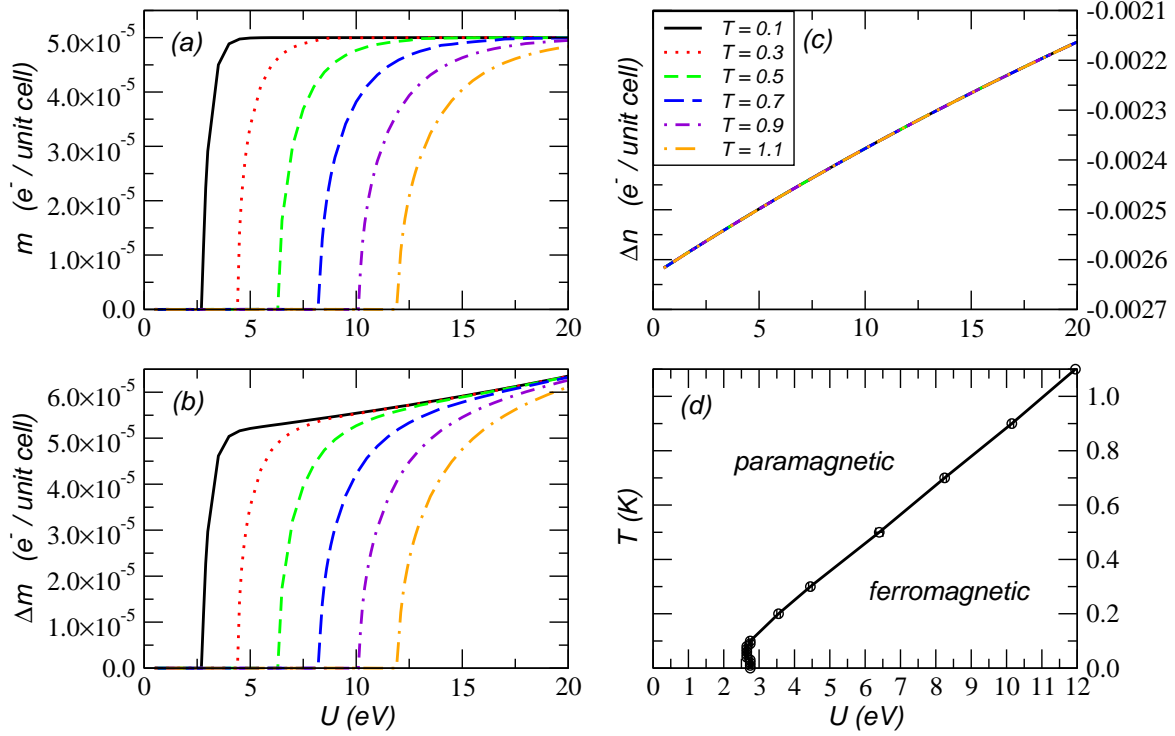


**Figure 7.** (Color online) Panels (a), (b), and (c) show the finite temperature self-consistent solution for  $m$ ,  $\Delta m$ , and  $\Delta n$ , respectively, with temperature measured in K. The finite temperature phase diagram of the biased bilayer in the  $U$  vs.  $T$  plane is shown in panel (d). The constant parameters are  $V = 0.05$  eV,  $t_{\perp} = 0.2t$ ,  $t = 2.7$  eV, and  $\delta n = 0.00005$   $e^-$ /unit cell.

opposite.

We note, however, that the cases  $U \gtrsim U_c$  and  $U \gg U_c$  mentioned above are parameter dependent. For instance, the valence bands can show an appreciable degeneracy lifting already for  $U \gtrsim U_c$ , especially for small values of the  $t_{\perp}$  parameter ( $t_{\perp} \lesssim 0.05t$ ). In this case the magnetization of the two layers is no longer opposite, with  $\Delta m < m$ . This can be understood as due to the fact that as  $t_{\perp}$  is decreased the weight of near-gap wave functions becomes more evenly distributed between layers, leading not only to a decrease in  $\Delta n$  but also in  $\Delta m$ . As  $U$  is further increased the energy splitting between *up* and *down* spin polarized bands gets larger, enhancing  $\Delta m$ . For  $U \gg U_c$ , and depending on the parameters  $V$  and  $t_{\perp}$ , the magnetization of the two layers may become opposite even for small  $t_{\perp}$  values.

#### 4.2. Finite temperature

Next we want to describe the phase diagram of the bilayer in the temperature vs. on-site Coulomb interaction  $U$  plane. This is done in Fig. 7 for a charge density  $\delta n = 5 \times 10^{-5}$  electrons per unit cell. For temperatures ranging from zero to  $T = 1.1$  K we studied the dependence of  $m$ ,  $\Delta m$  and  $\Delta n$  on the Coulomb on-site interaction  $U$ . First we note that the minimum critical value  $U_c$  is not realized at zero temperature. There is a reentrant

behavior which is signaled by the smallest  $U_c$  for  $T = 0.06 \pm 0.02$  K. For temperatures above  $T \approx 0.1$  K we have larger  $U_c$  values for the larger temperatures, as can be seen in panel (a). The same is true for  $\Delta m$ , panel (b). As in the case of Fig. 4, the value of  $\Delta m$ , at a given temperature and  $U$  value, is larger than  $m$ . Also the value of  $\Delta n$ , shown in panel (c), is larger than  $\delta n$ . Therefore we have the two planes presenting opposite magnetization and the charge carriers being hole like in one graphene plane and electron like in the other plane. In panel (d) of Fig. 7 we present the phase diagram in the  $T$  vs.  $U$ . Except at very low temperatures, there is a linear dependence of  $T$  on  $U_c$ . It is clear that at low temperatures,  $T \simeq 0.2$  K, the value of  $U_c$  is smaller than the estimated values of  $U$  for carbon compounds.[51, 52]

### 4.3. Disorder

Crucial prerequisite in order to find ferromagnetism is a high DOS at the Fermi energy. The presence of disorder will certainly cause a smoothing of the singularity in the DOS and the band gap renormalization, and can even lead to the closing of the gap. We note, however, that for small values of the disorder strength the DOS still shows an enhanced behavior at the band gap edges.[53, 54] The strong suppression of electrical noise in bilayer graphene[55] further suggests that in addition to a high crystal quality – leading to remarkably high mobilities[56] – an effective screening of random potentials is at work. Disorder should thus not be a limiting factor in the predicted low density ferromagnetic state, as long as standard high quality BLG samples are concerned.

Let us also comment on the next-nearest interlayer-coupling  $\gamma_3$ , which in the unbiased case breaks the spectrum into four pockets for low densities.[8] In the biased case,  $\gamma_3$  still breaks the cylindrical symmetry, leading to the trigonal distortion of the bands, but the divergence in the density of states at the edges of the band gap is preserved.[54] Therefore, the addition of  $\gamma_3$  to the model does not qualitatively change our result.

## 5. Summary

We have investigated the tendency of a biased bilayer graphene towards a ferromagnetic ground state. For this, we used a mean-field theory which allowed for a different carrier density and magnetization in the two layers. We have found that in the ferromagnetic phase the two layers have unequal magnetization and that the electronic density is hole like in one plane and electron like in the other. We have also found that at zero temperature, where the transition can be driven by doping, the phase transition between paramagnetic and ferromagnetic phases is *first-order*.

## Acknowledgments

TS, EVC, and NMRP acknowledge the financial support from POCI 2010 via project PTDC/FIS/64404/2006, and the financial support of Fundação para a Ciência e a



Tecnologia through Grant No. SFRH/BD/13182/2003. Support from ESF via INSTANS is also acknowledged.

## 6. References

- [1] A. K. Geim and K. S. Novoselov. The rise of graphene. *Nat. Mater.*, 6:183–191, 2007.
- [2] M. I. Katsnelson. Graphene: carbon in two dimensions. *Mater. Today*, 10:20–27, 2007.
- [3] A. H. Castro Neto, F. Guinea, and N. M. R. Peres. Drawing conclusions from graphene. *Physics World*, 19:33, 11 2006.
- [4] K.S. Novoselov, A.K. Geim, S.V. Morozov, D. Jiang, Y. Zhang, S.V. Dubonos, I.V. Grigorieva, and A.A. Firsov. Electric field effect in atomically thin carbon films. *Science*, 306:666, 2004.
- [5] K. S. Novoselov, D. Jiang, F. Schedin, T. J. Booth, V. V. Khotkevich, S. V. Morozov, and A. K. Geim. Two-dimensional atomic crystals. *Proc. Natl. Acad. Sci. U.S.A.*, 102:10451, 2005.
- [6] K.S. Novoselov, A.K. Geim, S.V. Morozov, D. Jiang, M.I. Katsnelson, I.V. Grigorieva, S.V. Dubonos, and A.A. Firsov. Two-dimensional gas of massless dirac fermions in graphene. *Nature*, 438:197, 2005.
- [7] Yuanbo Zhang, Yan-Wen Tan, Horst L. Stormer, and Philip Kim. Experimental observation of the quantum hall effect and berry’s phase in graphene. *Nature*, 438:201–204, 2005.
- [8] E. McCann and Vladimir I. Fal’ko. Landau-level degeneracy and quantum hall effect in a graphite bilayer. *Phys. Rev. Lett.*, 96:086805, 2006.
- [9] K. S. Novoselov, E. McCann, S. V. Morozov, V. I. Falko, M. I. Katsnelson, U. Zeitler, D. Jiang, F. Schedin, and A. K. Geim. Unconventional quantum hall effect and berry’s phase of  $2\pi$  in bilayer graphene. *Nature Phys.*, 2:177–180, 2006.
- [10] A. C. Ferrari, J. C. Meyer, V. Scardaci, C. Casiraghi, Michele Lazzeri, Francesco Mauri, S. Piscanec, Da Jiang, K. S. Novoselov, S. Roth, and A. K. Geim. The raman fingerprint of graphene. *Phys. Rev. Lett.*, 97:187401, 2006.
- [11] D. Graf, F. Molitor, K. Ensslin, C. Stampfer, A. Jungen, C. Hierold, and L. Wirtz. Spatially resolved raman spectroscopy of single- and few-layer graphene. *Nano Lett.*, 7:238, 2007.
- [12] Taisuke Ohta, Aaron Bostwick, Thomas Seyller, Karsten Horn, and Eli Rotenberg. Controlling the electronic structure of bilayer graphene. *Science*, 313:951, 2006.
- [13] Eduardo V. Castro, K. S. Novoselov, S. V. Morozov, N. M. R. Peres, J. M. B. Lopes dos Santos, Johan Nilsson, F. Guinea, A. K. Geim, and A. H. Castro Neto. Biased bilayer graphene: semiconductor with a gap tunable by electric field effect. *Phys. Rev. Lett.*, 99:216802, 2007.
- [14] F. Guinea, A. H. Castro Neto, and N. M. R. Peres. Electronic states and landau levels in graphene stacks. *Phys. Rev. B*, 73:245426, 2006.
- [15] Jeroen B. Oostinga, Hubert B. Heersche, Xinglan Liu, Alberto F. Morpurgo, and Lieven M. K. Vandersypen. Gate-induced insulating state in bilayer graphene devices. *Nature Mater.*, 7:151 – 157, 2007.
- [16] Claire Berger, Zhimin Song, Tianbo Li, Xuebin Li, Asmerom Y. Ogbazghi, Rui Feng, Zhenting Dai, Alexei N. Marchenkov, Edward H. Conrad, Phillip N. First, and Walt A. de Heer. Ultrathin epitaxial graphite: 2d electron gas properties and a route toward graphene-based nanoelectronics. *J. Phys. Chem.*, 108:19912, 2004.
- [17] P. Esquinazi, A. Setzer, R. Höhne, C. Semmelhack, Y. Kopelevich, D. Spemann, T. Butz, B. Kohlstrunk, and M. Lösche. Ferromagnetism in oriented graphite samples. *Phys. Rev. B*, 66:024429, 2002.
- [18] H. Kempa, P. Esquinazi, and Y. Kopelevich. Field-induced metal-insulator transition in the c-axis resistivity of graphite. *Phys. Rev. B*, 65:241101, 2002.
- [19] H. Kempa, H. C. Semmelhack, P. Esquinazi, and Y. Kopelevich. Absence of metal–insulator transition and coherent interlayer transport in oriented graphite in parallel magnetic fields. *Sol. State Commun.*, 125:1, 2003.

- [20] Y. Kopelevich, J. H. S. Torres, R. R. da Silva, F. Mrowka, H. Kempa, and P. Esquinazi. Reentrant metallic behavior of graphite in the quantum limit. *Phys. Rev. Lett.*, 90:156402, 2003.
- [21] H. Ohldag, T. Tyliczszak, R. Höhne, D. Spemann, P. Esquinazi, M. Ungureanu, and T. Butz.  $\pi$ -Electron Ferromagnetism in Metal-Free Carbon Probed by Soft X-Ray Dichroism. *Phys. Rev. Lett.*, 98:187204, 2007.
- [22] A. V. Rode, E. G. Gamaly, A. G. Christy, J. G. Fitz Gerald, S. T. Hyde, R. G. Elliman, B. Luther-Davies, A. I. Veinger, J. Androulakis, and J. Giapintzakis. Unconventional magnetism in all-carbon nanofoam. *Phys. Rev. B*, 70:054407, 2004.
- [23] Philippe Turek, Kiyokazu Nozawa, Daisuke Shiomi, Kunio Awaga, Tamotsu Inabe, Yusei Maruyama, and Minoru Kinoshita. Ferromagnetic coupling in a new phase of the p-nitrophenyl nitronyl nitroxide radical. *Chem. Phys. Lett.*, 180:327, 1991.
- [24] V. I. Srdanov, G. D. Stucky, E. Lippmaa, and G. Engelhardt. Evidence for an antiferromagnetic transition in a zeolite-supported cubic lattice of f centers. *Phys. Rev. Lett.*, 80:2449 – 2452, 1998.
- [25] Toshiaki Enoki and Yousuke Kobayashi. Magnetic nanographite: an approach to molecular magnetism. *J. Mater. Chem.*, 15:3999 – 4002, 2005.
- [26] Alexandr A. Ovchinnikov. Multiplicity of the ground state of large alternant organic molecules with conjugated bonds. *Theor. Chem. Acta*, 47:297, 1978.
- [27] A. A. Ovchinnikov and I. L. Shamovsky. The structure of the ferromagnetic phase of carbon. *Shamovsky, J. Mol. Structure (Theochem)*, 251:133, 1991.
- [28] T. Stauber, F. Guinea, and M. A. H. Vozmediano. Disorder and interaction effects in two-dimensional graphene sheets. *Phys. Rev. B*, 71:041406(R), 2005.
- [29] M. A. H. Vozmediano, M. P. López-Sancho, T. Stauber, and F. Guinea. Local defects and ferromagnetism in graphene layers. *Phys. Rev. B*, 72:155121, 2005.
- [30] Mitsutaka Fujita, Katsunori Wakabayashi, Kyoko Nakada, and Koichi Kusakabe. Peculiar localized state at zigzag graphite edge. *J. Phys. Soc. Jpn.*, 65:1920–1923, 1996.
- [31] L. Pisani, J. A. Chan, B. Montanari, and N. M. Harrison. Electronic structure and magnetic properties of graphitic ribbons. *Phys. Rev. B*, 75:064418, 2007.
- [32] A Mielke. Ferromagnetic ground states for the hubbard model on line graphs. *J. Phys. A: Math. Gen.*, 24:L73–L77, 1991.
- [33] Hal Tasaki. From nagaoka’s ferromagnetism to flat-band ferromagnetism and beyond — an introduction to ferromagnetism in the hubbard model —. *Prog. Theor. Phys.*, 99:489, 1998.
- [34] Koichi Kusakabe and Masanori Maruyama. Magnetic nanographite. *Phys. Rev. B*, 67:092406, 2003.
- [35] B. Wunsch, T. Stauber, and F. Guinea. Electron-electron interaction and charging effects in a graphene quantum dot. *Phys. Rev. B*, 77:035316, 2008.
- [36] B. Wunsch, T. Stauber, F. Sols, and F. Guinea. Interactions and magnetism in graphene boundary states. *Phys. Rev. Lett. [in press]*, 2008. arXiv:0803.1050.
- [37] J. A. Chan, B. Montanari, J. D. Gale, S. M. Bennington, J. W. Taylor, and N. M. Harrison. Magnetic properties of polymerized c60 : The influence of defects and hydrogen. *Phys. Rev. B*, 70:041403(R), 2004.
- [38] Tatiana Makarova and Fernando Palacio, editors. *Carbon Based Magnetism: An Overview of the Magnetism of Metal Free Carbon-based Compounds and Materials*. Elsevier, Amsterdam, 2006.
- [39] N. M. R. Peres, M. A. N. Araújo, and Daniel Bozi. Phase diagram and magnetic collective excitations of the hubbard model for graphene sheets and layers. *Phys. Rev. B*, 70:195122, 2004.
- [40] M. A. N. Araújo and N. M. R. Peres. Weak ferromagnetism and spiral spin structures in honeycomb hubbard planes. *J. Phys.: Condens. Matter*, 18:1769–1779, 2006.
- [41] N. M. R. Peres, F. Guinea, and A. H. Castro Neto. Coulomb interactions and ferromagnetism in pure and doped graphene. *Phys. Rev. B*, 72:174406, 2005.
- [42] N. M. R. Peres, F. Guinea, and A. H. Castro Neto. Electronic properties of disordered two-

- dimensional carbon. *Phys. Rev. B*, 73:125411, 2006.
- [43] Vitor M. Pereira, F. Guinea, J. M. B. Lopes dos Santos, N. M. R. Peres, and A. H. Castro Neto. Disorder induced localized states in graphene. *Phys. Rev. Lett.*, 96:036801, 2006.
- [44] Oleg V. Yazyev and Lothar Helm. Defect-induced magnetism in graphene. *Phys. Rev. B*, 75:125408, 2007.
- [45] Johan Nilsson, A. H. Castro Neto, N. M. R. Peres, and F. Guinea. Electron-electron interactions and the phase diagram of a graphene bilayer. *Phys. Rev. B*, 73:214418, 2006.
- [46] T. Stauber, N. M. R. Peres, F. Guinea, and A. H. Castro Neto. Fermi liquid theory of a fermi ring. *Phys. Rev. B*, 75:115425, 2007.
- [47] Eduardo V. Castro, N. M. R. Peres, T. Stauber, and N. A. P. Silva. Low density ferromagnetism in a biased bilayer graphene. *Phys. Rev. Lett.*, page 186803, 2008.
- [48] Assuming equal spin densities in sublattices  $A$  and  $B$  of the same layer is a reasonable approximation for  $t_{\perp} \ll t$ .
- [49] Edward McCann. Asymmetry gap in the electronic band structure of bilayer graphene. *Phys. Rev. B*, 74:161403, 2006.
- [50] Hongki Min, B.R. Sahu, Sanjay K. Banerjee, and A.H. MacDonald. Ab initio theory of gate induced gaps in graphene bilayers. *Phys. Rev. B*, 75:155115, 2007.
- [51] Robert G. Parr, David P. Craig, and Ian G. Ross. Molecular orbital calculations of the lower excited electronic levels of benzene, configuration interaction included. *J. Chem. Phys.*, 18:1561–1563, 1950.
- [52] Dionys Baeriswyl, David K. Campbell, and Sumit Mazumdar. Correlations and defect energies. *Phys. Rev. Lett.*, 56:1509 – 1509, 1986.
- [53] Johan Nilsson and A. H. Castro Neto. Impurities in a biased graphene bilayer. *Phys. Rev. Lett.*, 98:126801, 2007.
- [54] Johan Nilsson, A. H. Castro Neto, F. Guinea, and N. M. R. Peres. Electronic properties of bilayer and multilayer graphene. arXiv:0712.3259v2 [cond-mat.mes-hall].
- [55] Yu-Ming Lin and Phaeton Avouris. Strong suppression of electrical noise in bilayer graphene nano devices. *ASAP Nano Lett.*, 2008. doi:10.1021/nl080241l.
- [56] S.V. Morozov, K.S. Novoselov, M.I. Katsnelson, F. Schedin, D. Elias, J.A. Jaszczak, and A.K. Geim. Giant intrinsic carrier mobilities in graphene and its bilayer. *Phys. Rev. Lett.*, 100:016602, 2008.